

UNSUPERVISED BODY PART REGRESSION USING CONVOLUTIONAL NEURAL NETWORK WITH SELF-ORGANIZATION

Ke Yan, Le Lu, Ronald M. Summers

Imaging Biomarkers and Computer-Aided Diagnosis Laboratory
 Radiology and Imaging Sciences Department
 National Institutes of Health Clinical Center
 Bethesda, MD 20892, USA

ABSTRACT

Automatic body part recognition for CT slices can benefit various medical image applications. Existing methods require large-scale datasets of labeled images. However, the intrinsic structure information in CT volumes was still not fully leveraged. In this paper, we propose unsupervised body part regressor (UBR) to utilize this information. A novel learning framework based on a convolutional neural network and two inter-sample loss functions was designed. UBR builds a coordinate system for the body and outputs a continuous score for each slice, which represents the normalized position of the body part in the slice. The training process of UBR resembles a self-organization process: slice scores are learned from inter-slice relationships. The training samples are unlabeled volumes that are abundant in every hospital’s database, thus zero annotation effort is needed. UBR is simple, fast, and accurate. Qualitative and quantitative experiments proved its effectiveness. Besides, we show potential applications of UBR in network initialization and anomaly detection.

Index Terms— Body Part Recognition, CNN, Unsupervised Learning, Self-Organize, Slice Order

1. INTRODUCTION

Body part recognition is useful in many medical image applications, such as automatic scan range planning and image preprocessing, initialization of other computer aided detection (CADe) and diagnosis (CADx) systems, content-based medical image retrieval, and so on [1]. Traditional methods often use hand-crafted features to train classifiers [1]. Lately, deep learning approaches [1, 2, 3] have been widely adopted with promising results. They rely on convolutional neural networks (CNNs) to learn high-level features. However, a large set of labeled training data are required. Recently, Zhang et al. [3] proposed a self-supervised method which pretrains a CNN in an unsupervised manner. Nevertheless, it still needs

fine-grained labeled volumes to fine-tune the network before predicting body parts.

In this paper, we present an Unsupervised Body part Regressor (UBR) that purely learns from unlabeled volumes. The training volumes can have any scan range (chest, abdomen, pelvis, ...), hence are abundant in every hospital’s picture archiving and communication system (PACS). The slice order information is leveraged to train UBR. This intuition resembles [3] but our training procedure, network structure, and loss function are all different. UBR is more efficient, accurate, and requires no labeled training samples. By minimizing an order loss and a distance loss, UBR learns body part knowledge from inter-slice relationships in a way analogous to a self-organization process, which is defined as “some overall order arises from local interactions between parts of an initially disordered system” (Wikipedia).

Most previous works split the whole body into several discrete parts [1, 2], which is somehow arbitrary. The algorithms will be problematic at transition regions [2]. Furthermore, they cannot discriminate slices inside a part. On the other hand, UBR is a regressor. It builds a coordinate system for the body and outputs a continuous score for each slice, which represents the normalized position of the body part in the slice. Thus, it is fine-grained and useful for all researchers who focus on different parts of the body. Experimental results show that it outperforms ref. [3] which used 88 extra labeled volumes to fine-tune. UBR’s end-to-end training process requires only 12 min to converge. Besides body part recognition, we demonstrate two potential applications of UBR: initialization of the weights in a CNN for other medical image and detection of significant anomalies in volumes, such as scan artifacts or large lesions.

2. METHOD

2.1. Motivation

Medical images are intrinsically structured. The position and appearance of organs are relatively fixed, so one algorithm should be able to learn concepts of body parts by looking at a

batch of unlabeled volumes, as long as a good learning strategy can be designed. Our final goal is to predict a continuous score for each axial slice which represents the normalized coordinate of the body part. As the slice indices in a volume increase, the slice scores should also increase. Note that the volumes mined from PACS often have different scan ranges (including start, end, and slice intervals). Therefore, we cannot directly use the slice indices as slice scores or as labels to learn the scores.

However, we know that a slice with a larger index should have a larger score. In addition, the difference in slice scores should be roughly proportional to the difference in slice indices, assuming that the slice intervals are constant and inter-subject variance of body parts is small. Following this intuition, we propose the unsupervised body part regressor (UBR), see Fig. 1.

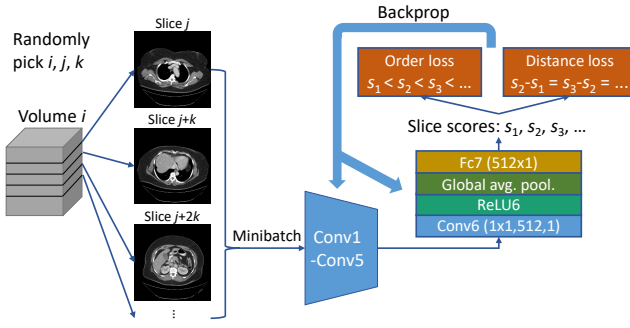


Fig. 1. Framework of the proposed unsupervised body part regressor (UBR).

2.2. Selection of training samples

In each iteration of training, we randomly select g volumes, then randomly pick m equidistant slices from each volume. A starting slice j and a selection interval k are randomly determined (Fig. 1), then m equidistant slices can be chosen. One problem is that the selection strategy makes slices in the middle of a volume more likely to be chosen. We can fix this problem by increasing the probability for slices at both ends.

2.3. Network structure

For each training or test slice, we use a CNN to generate its score, as shown in Fig. 1. The first few layers of the network include convolution, rectified linear unit (ReLU), and max pooling. They can be copied from popular CNNs, e.g. the conv1-conv5 in AlexNet [4] and VGG-16 [5]. Then, we add a new convolutional layer, Conv6, with 512×1 filters and stride 1, followed by a ReLU layer. Conv1-Conv6 are used to learn discriminative features for body part recognition. After that, a global average pooling layer is attached to

summarize each of the 512 activation maps to one value, leading to a 512D feature vector. It makes the network robust to the position of the body in the slice. Finally, a fully connected layer (Fc7) projects the feature vector to the slice score.

2.4. Loss function

The loss function is key in this unsupervised method. Because labels are not available, we try to learn the relationship between slice scores instead of fitting the scores directly. A similar idea is introduced in the Siamese network [6], but we have extended it by using more than two samples as a group and adopting two inter-subject loss terms. Experimental results in Section 3 will show the superiority of these strategies.

The first loss term is the order loss L_{order} , which requires slices with larger indices to have larger scores. As expressed in Eq. 1, L_{order} is a logistic loss. g is the number of volumes in a minibatch; m is the number of slices in each volume; $S(i, j)$ is the slice score of slice j in volume i ; h is the sigmoid function.

$$L_{\text{order}} = - \sum_{i=1}^g \sum_{j=1}^{m-1} \log h(S(i, j+1) - S(i, j)). \quad (1)$$

Besides keeping the order of the slice scores, we also hope to make them increase linearly. The difference between two slice scores should be proportional to the physical distance between the two slices. Because we intentionally pick equidistant slices (e.g. slices $j, j+k, j+2k, \dots$), the slice scores should be equidistant, too. The distance loss is thus defined as:

$$L_{\text{dist}} = \sum_{i=1}^g \sum_{j=1}^{m-2} f(\Delta_{i,j+2} - \Delta_{i,j+1}), \quad (2)$$

$$\Delta_{i,j} = S(i, j) - S(i, j-1),$$

where f is the smooth L1 loss [7]. The final loss is

$$L = L_{\text{order}} + L_{\text{dist}}. \quad (3)$$

In the training process, the order loss and the distance loss collaborate to “push” each slice score towards the correct direction relative to other slices. If the order loss does not exist, a trivial solution will be obtained and all slice scores will be constant. If the distance loss is absent, the slice scores will be nonlinear and less accurate.

3. EXPERIMENTS

3.1. Dataset and implementation details

To evaluate the proposed algorithm, we collected 800 unlabeled CT volumes of 420 subjects from the PACS of our hospital. There are about 30–700 slices in each volume. They were used as the training set of UBR. Most volumes

are chest-abdomen-pelvis scans, but we do not know the exact scan range of each volume during training. The test set includes 18195 slices subsampled from 260 new volumes of 140 new subjects. Each slice was manually labeled as one of the 3 classes: chest (5903 slices), abdomen (6744), or pelvis (5548). In this dataset, the abdomen class starts from the upper border of the liver and ends at the upper border of the ilium. We only annotated three classes because most data are in this range. However, the proposed method can be easily extended to other parts of the body. Note that all training and test volumes were arbitrarily chosen. They have different pixel spacing (0.6–1.0 mm) and a variety of pathological conditions.

The slices were resized to 128×128 pixels. No further preprocessing or data augmentation was performed. As shown in Fig. 1, the layers Conv1–Conv5 of UBR were the same as those in VGG-16 [5]. They were initialized using the ImageNet [8] pretrained model. Conv6 and Fc7 were randomly initialized. We set the number of volumes per mini-batch $g = 12$ and the number of slices per volume $m = 8$. The network was trained using stochastic gradient descent with initial learning rate 0.002 and converged in 1.5K iterations, taking only 12 min on a Titan X Pascal GPU. The inference time for each slice is 4 ms.

3.2. Qualitative and quantitative results

We found the learned slice scores mostly ranged between -15 and 15. Fig. 2 illustrates some qualitative results. It can be found that scores and body parts have a clear correspondence (-10: upper chest, -5: liver dome, 0: lower abdomen, 5: lower pelvis). UBR is robust to variance in position, size, and pathological conditions (row 1 column 1, atypical presentation of bowel in the chest) of the body. Besides, Fig. 2 shows potential application of UBR on content-based image retrieval from PACS.

To evaluate the performance of UBR, we classified the test slices into three classes based on the slice scores. Two extra volumes were used to determine two thresholds for the slice scores. We also implemented two existing methods for comparison. The first method directly trains a 3-class classifier based on labeled slices, which is similar to [2]. The second method is the self-supervised method in [3]. It first pretrains the network with unlabeled slice pairs, then fine-tunes with fine-grained labeled volumes to learn slice scores. In the pre-training stage, it concatenates the Fc6 features of two slices to predict the order relationship between the slices. Thus, it cannot directly generate slice scores or use the multi-slice order loss or distance loss. We calibrate two threshold scores for it like UBR. Both [2] and [3] require labeled samples in training, so we further manually annotated 88 volumes from 88 new subjects. Both methods use AlexNet as the backbone structure. The results are displayed in Table 1.

The supervised classifier [2] achieved the highest accu-

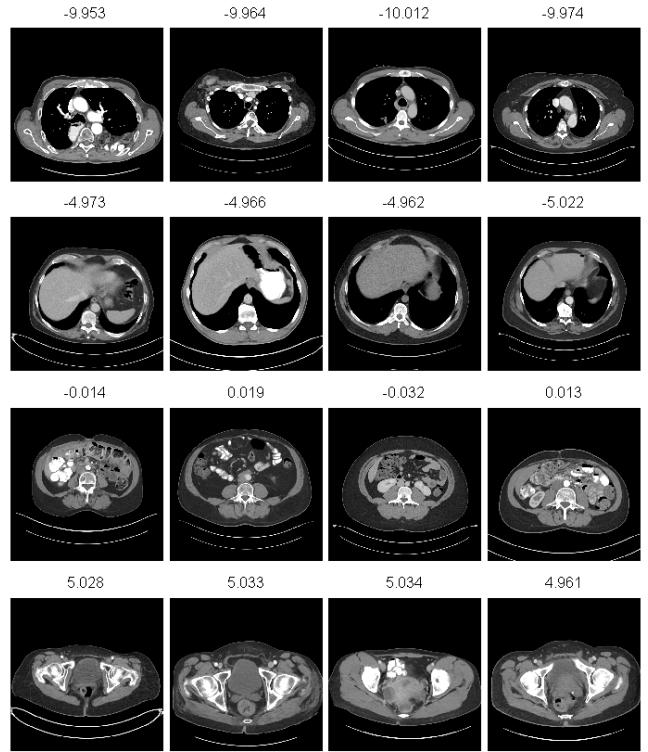


Fig. 2. Sample slices with slice scores close to -10, -5, 0, and 5, respectively. Slices in the same row have similar scores as well as body parts. They were randomly picked from the test set. The numbers above each slice are slice scores.

Method	Acc. (%)
Supervised [2] with 88 labeled volumes	98.84
Self-supervised [3] with 88 labeled volumes	95.28
Self-supervised [3] with 2 labeled volumes	72.05
UBR with 2 labeled volumes	95.99
UBR (AlexNet) with 2 labeled volumes	95.61
UBR, pool6 features with 88 labeled volumes	98.41

Table 1. Accuracy comparison for body part classification.

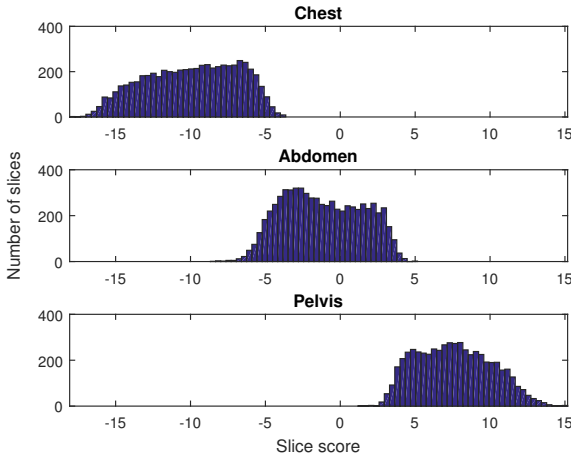


Fig. 3. Histogram of slice scores in each class in the test set.

racy, which is higher than the result in [2] because the labels in our dataset are purer and we used fewer classes. However, this method needs labeled volumes for training. In addition, it is dedicated to classification, which is an easier task than fine-grained regression in [3] and UBR. Using only 2 labeled volumes to calibrate thresholds, UBR outperformed the self-supervised method [3] which fine-tuned with 88 labeled volumes. For fair comparison, we also tested UBR with AlexNet backbone, which is still better than [3]. The accuracy of fine-tuning the network of [3] with two labeled volumes is poor because of overfitting. Finally, we explored using the 512D feature vector from pool6 of UBR to train a logistic regression classifier on the 88 labeled volumes without fine-tuning UBR. An improved accuracy can be observed. The pool6 features contain information related to body parts, therefore can be directly used to train a better classifier when labeled samples are presented. It will be interesting to see if they can also be applied to train classifiers in other CADx tasks.

To analyze the errors of UBR, we draw the histogram of slice scores in each class in Fig. 3. It can be found that most classification errors appear at transition regions because of their ambiguity. Actually, this is not a problem when UBR is applied in practice since it predicts continuous scores. Besides, we observed that the scores for certain body parts may not be accurate if the unlabeled training dataset contains few samples on this part. This is understandable. It can be fixed by simply collecting more related volumes.

Incorporating the distance loss and choosing a proper m can improve the body part recognition accuracy, as indicated by Fig. 4. When increasing m , we also decreased g to keep $m \times g = 96$. If $m = 2$, the distance loss cannot be applied and the order loss is the same with [3]. Its result is inferior than those with $m > 2$, proving the effectiveness of the proposed multi-slice strategy. With more slices per group, the inter-slice relationship can be better regulated, especially when the

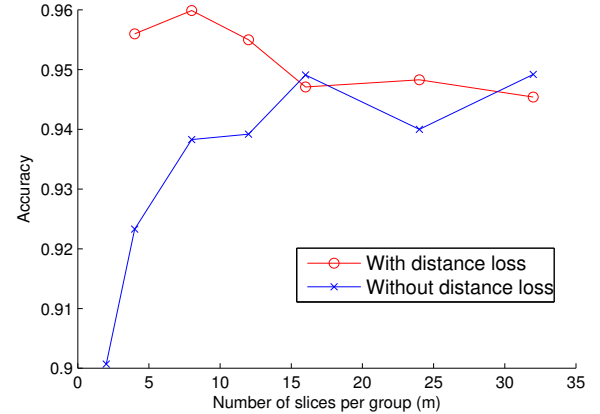


Fig. 4. Accuracy of body part classification of UBR with different parameters.

distance loss is absent. The distance loss can also improve the accuracy. But when there are too many slices per group, the constraint of the distance loss may be so strict that it can harm the accuracy.

3.3. Application: network initialization

Transfer learning is important for CNN-based medical image applications. Because medical datasets are often small compared to the huge amount of parameters in CNNs, training a CNN from scratch is difficult. Many researches have found that initializing the network weights with ImageNet pretrained models significantly improves accuracy [9, 10]. However, there is a gap between the statistics of natural and medical images. In this section, we explore the feasibility of using UBR's model to help the initialization of CNNs for other CAD tasks.

The new CAD task in this section is lesion detection on a large-scale dataset called DeepLesion, which was collected by our lab. It contains 32120 CT slices of size 512×512 from 10594 studies of 4459 unique patients. There are bounding-boxes annotated by radiologists on each slice, marking a variety of lesions including lung nodules, lymph nodes, liver/kidney lesions, and so on. We adopted Faster RCNN [7] with VGG-16 backbone to detect the lesions regardless of their types (lesion vs. non-lesion). To match the UBR model with this task, we changed the image size to 512×512 when training UBR.

We explored four initialization strategies for DeepLesion: Random (training a Faster RCNN from scratch), UBR (using a UBR model trained from scratch to initialize Faster RCNN), ImageNet (using a VGG-16 model trained on ImageNet to initialize Faster RCNN), and ImageNet+UBR (first using an ImageNet model to initialize UBR, then using the UBR to initialize Faster RCNN). It is worth mentioning that the UBR model trained from scratch obtained comparable accuracy on

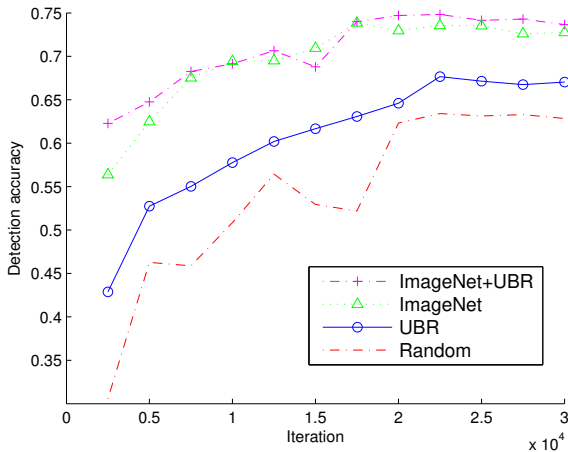


Fig. 5. Detection accuracy with different initialization methods on the validation set of the DeepLesion dataset. The x -axis is the training iteration.

body part classification to the one with ImageNet initialization, which is because the unlabeled training slices are abundant. The learning rates of each strategy was adjusted according to the convergence speed. They started from 0.002 and were reduced by a factor of 10 in every 20K, 20K, 15K, and 15K iterations, respectively. The detection accuracy on DeepLesion is exhibited in Fig. 5. The accuracy is the average recall of top-5 detections on each slice. A predicted box is treated as correct if the intersection-over-union between it and a ground-truth box is larger than 0.5.

We can find that initializing the detector with the UBR model is better than training it from scratch, because filters learned in UBR can benefit the detector. It indicates that UBR can be utilized to initialize CNNs when ImageNet pretrained models are not available. However, the ImageNet pretrained model still outperforms the UBR pretrained one, which is because ImageNet is a much larger and labeled dataset. The pretrained model learned all kinds of filters from it, especially those for fine textures, therefore is more suitable for detecting small lesions. On the other hand, the double pretrain strategy (ImageNet+UBR) achieved a higher initial accuracy (at 2.5K and 5K iterations) and a slightly improved final accuracy (74.82% vs. 73.84%). The probable reason is that UBR can familiarize the CNN with the statistics of CT images, meanwhile keep the useful filters learned from ImageNet, thus initialize the network in a better starting point.

3.4. Application: anomaly detection

UBR can also be used to mine slices with significant abnormal appearance, in other words, those that are rare in the training set, such as scan artifacts and large lesions. A simple method is to calculate the scores for all slices in a volume then plot them against the slice indices to get a slice score curve. In

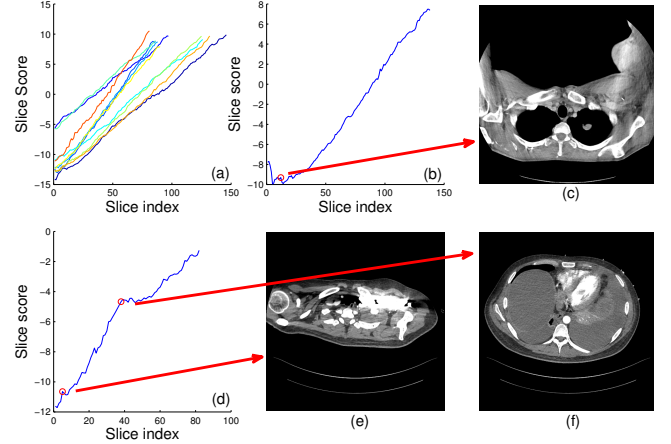


Fig. 6. Example of anomaly detection using UBR. (a). Slice score curves in 10 normal volumes. (b)–(f). Slice score curves and sample slices in two abnormal volumes.

normal volumes (Fig. 6 (a)), the curves are roughly linear with small noises indicating inter-subject variances. The initial and final values of each curve suggest the scan range of the volume. Then, we compute the correlation coefficient (r) between slice indices and slice scores. Fig. 6 (b) and (d) are two sample volumes with $r < 0.99$. By manually examining the slices, we found that the nonlinearity in the beginning of the first volume is caused by the atypical position of the patient’s arm (Fig. 6 (c)), whereas those in the second volume are respectively due to the abnormal distribution of contrast and pleural and ascitic fluid in chest and abdomen (Fig. 6 (e) and (f)).

4. CONCLUSION

In this paper, we proposed an Unsupervised Body part Regressor (UBR) that learns a normalized coordinate system for body parts based on unlabeled volumes. It is simple and effective, with zero annotation effort needed. Experiments have been conducted on axial CT slices, but UBR may also be extended to coronal and sagittal slices to learn 3D slice scores.

5. REFERENCES

- [1] Zhennan Yan, Yiqiang Zhan, Zhigang Peng, Shu Liao, Yoshihisa Shinagawa, Shaotong Zhang, Dimitris N Metaxas, and Xiang Sean Zhou, “Multi-instance deep learning: Discover discriminative local anatomies for bodypart recognition,” *IEEE transactions on medical imaging*, vol. 35, no. 5, pp. 1332–1343, 2016.
- [2] Holger R Roth, Christopher T Lee, Hoo-Chang Shin, Ari Seff, Lauren Kim, Jianhua Yao, Le Lu, and Ronald M Summers, “Anatomy-specific classification

of medical images using deep convolutional nets,” in *Biomedical Imaging (ISBI), 2015 IEEE 12th International Symposium on*. IEEE, 2015, pp. 101–104.

- [3] Pengyue Zhang, Fusheng Wang, and Yefeng Zheng, “Self supervised deep representation learning for fine-grained body part recognition,” in *Proc. of 2017 IEEE International Symposium on Biomedical Imaging*, Melbourne, Australia, 2017.
- [4] Alex Krizhevsky, Ilya Sutskever, and Geoffrey E Hinton, “Imagenet classification with deep convolutional neural networks,” in *Advances in neural information processing systems*, 2012, pp. 1097–1105.
- [5] Karen Simonyan and Andrew Zisserman, “Very deep convolutional networks for large-scale image recognition,” in *ICLR 2015*, 2015.
- [6] Jane Bromley, Isabelle Guyon, Yann LeCun, Eduard Säckinger, and Roopak Shah, “Signature verification using a “siamese” time delay neural network,” in *Advances in Neural Information Processing Systems*, 1994, pp. 737–744.
- [7] Shaoqing Ren, Kaiming He, Ross Girshick, and Jian Sun, “Faster R-CNN: Towards real-time object detection with region proposal networks,” in *Advances in neural information processing systems*, 2015, pp. 91–99.
- [8] J Deng, W Dong, R Socher, L J Li, Kai Li, and Li Fei-Fei, “ImageNet: A large-scale hierarchical image database,” in *2009 IEEE Conference on Computer Vision and Pattern Recognition*, jun 2009, pp. 248–255.
- [9] Hayit Greenspan, Bram van Ginneken, and Ronald M Summers, “Guest editorial deep learning in medical imaging: Overview and future promise of an exciting new technique,” *IEEE Transactions on Medical Imaging*, vol. 35, no. 5, pp. 1153–1159, 2016.
- [10] Hoo-Chang Shin, Holger R Roth, Mingchen Gao, Le Lu, Ziyue Xu, Isabella Nogues, Jianhua Yao, Daniel Mollura, and Ronald M Summers, “Deep convolutional neural networks for computer-aided detection: CNN architectures, dataset characteristics and transfer learning,” *IEEE transactions on medical imaging*, vol. 35, no. 5, pp. 1285–1298, 2016.